Electronic Supplementary Information

Experimental Section

Materials: Sodium nitrate ($NaNO_3$, 99.0%), sodium nitrite ($NaNO_2$, 99.0%), ammonium chloride (NH_4Cl), sodium hydroxide (NaOH), sodium salicylate ($C_7H_5NaO_3$), trisodium citrate dihydrate ($C_6H_5Na_3O_7{\cdot}2H_2O$), p-dimethylaminobenzaldehyde ($C_9H_{11}NO$), sodium nitroferricyanide dihydrate ($C_5FeN_6Na_2O{\cdot}2H_2O$), 0.8 wt% sulfamic acid solution (H_3NO_3S), sodium dihydrogen phosphate dihydrate (NaH_2PO_4), disodium hydrogen phosphate dodecahydrate (Na_2HPO_4) and sodium hypochlorite solution (NaClO) were purchased from Aladdin Ltd. (Shanghai, China). Coblat acetate tetrahydrate [$Co(CH_3COO)_2{\cdot}4H_2O$], and ammonium chloride (NH_4Cl) were purchased from Chengdu Kelong Chemical Regent Co. Ltd. Sulfuric acid (H_2SO_4), hydrogen peroxide (H_2O_2), hydrochloric acid (HCl), hydrazine monohydrate ($N_2H_4{\cdot}H_2O$) and ethylalcohol (C_2H_5OH) were bought from Beijing Chemical Corporation. (China). chemical Ltd. in Chengdu. Carbon paper was purchased from Qingyuan Metal Materials Co., Ltd (Xingtai, China). All reagents used in this work were analytical grade without further purification.

Preparation of PP-Co: In brief, $Co(CH_3COO)_2{\cdot}4H_2O$ was dissolved in 30 mL ultrapure water with the different concentrations of 0.1 M, 0.05 M, and 0.01 M, respectively. Then add 0.3 g pretreatment pomelo peel. After standing still for 6 h, the soaked pomelo peels were taken out and washed with distilled water, followed by drying at 60 °C overnight. After drying the soaked pomelo peels, the soaked pomelo peels were calcined at 800 ℃ for 2 h with a temperature rate of 2 ℃ min^{-1} under argon atmosphere, the resulting products are named PP-Co-0.1, PP-Co, PP-Co-0.01, respectively. The pure PP was obtained without adding $Co(CH_3COO)_2{\cdot}4H_2O$.

Characterizations: XRD data were acquired by a LabX XRD-6100 X-ray diffractometer with a Cu Kα radiation (40 kV, 30 mA) of wavelength 0.154 nm (SHIMADZU, Japan). SEM measurements were carried out on a GeminiSEM 300 scanning electron microscope (ZEISS, Germany) at an accelerating voltage of 5 kV. XPS measurements were performed on an ESCALABMK II X-ray photoelectron

spectrometer using Mg as the exciting source. The absorbance data of spectrophotometer was measured on UV-Vis spectrophotometer. TEM image was obtained from a Zeiss Libra 200FE transmission electron microscope operated at 200 kV.

Electrochemical measurements: 10 mg of the catalyst and 40 μL of 5 wt% Nafion were dispersed in 960 μL of a deionized water/ethanol solution (v/v = 1:3) by sonicating for 2 h to get a homogeneous catalyst ink. Then, a certain volume of the ink was dropped onto a 1 × 1 cm carbon paper with a catalyst loading of 0.2 mg cm^{-2} and dried at room temperature. All electrochemical measurements were performed in a two-compartment cell separated by a treated Nafion 117 membrane using the CHI660E electrochemical workstation (Shanghai, Chenhua) with a standard three-electrode setup. Electrolyte solution was Ar-saturated 0.1 M NaOH with 0.1 M $NaNO_3$/$NaNO_2$, using PP-Co/CP (0.2 mg cm^{-2}) as the working electrode, a carbon rod as the counter electrode and a Hg/HgO as the reference electrode. All the potentials reported in our work were converted to reversible hydrogen electrode (RHE) scale via calibration with the following equation: E (RHE) = E (vs. Hg/HgO) + 0.0591 × pH + 0.098 V and the current density was normalized by the geometric surface area.

Determination of NH_3: Concentration of produced NH_3 was determined by spectrophotometry measurement with indophenol blue method (the obtained electrolyte was diluted 50 times).[1] In detail, 2 mL of the diluted catholyte was obatined from the cathodic chamber and mixed with 2 mL of a 1 M NaOH solution that contained salicylic acid and sodium citrate. Then, 1 mL of 0.05 M NaClO and 0.2 mL of 1 wt% $C_5FeN_6Na_2O$ were dropped in the collected electrolyte solution. After standing at room temperature for 2 h, the ultraviolet-visible absorption spectrum was measured. The concentration-absorbance curve was calibrated using the standard NH_4Cl solution with NH_3 concentrations of 0, 0.2, 0.5, 1.0, 2.0, 0.25, and 5.0 μg mL^{-1} in 0.1 M NaOH. The absorbance at 655 nm was measured to quantify the NH_3 concentration using standard NH_4Cl solutions ($y = 0.38775\ x + 0.05091$, $R^2 = 0.999$).

Determination of NO_2^-: Owing to the large concentration of solution, the obtained reaction solutions were diluted 50 times. The NO_2^- concentration was analyzed using the Griess test.[2] The Griess reagent was prepared by dissolving 0.1 g N-(1-naphthyl) ethylenediamine dihydrochloride, 1.0 g sulfonamide and 2.94 mL H_3PO_4 in 50 mL deionized water. In a typical colorimetric assay, the 1.0 mL Griess reagent was mixed with the 1.0 mL nitrite-containing solution and 2.0 mL H_2O, and allowed to react at room temperature for 10 min, in which sulfonamide reacts with NO_2^- to form a diazonium salt and then further reacts with amine to form an azo dye (magenta). The absorbance at 540 nm was measured to quantify the NO_2^- concentration with a standard curve of NO_2^- ($y = 0.20276\ x + 0.33532$, $R^2 = 0.999$).

Determination of N_2H_4: In this work, we used the method of Watt and Chrisp[3] to determined the concentration of produced N_2H_4. The chromogenic reagent was a mixed solution of 5.99 g $C_9H_{11}NO$, 30 mL HCl and 300 mL C_2H_5OH. In detail, 1 mL electrolyte was added into 1 mL prepared color reagent and stirred for 15 min in the dark. The absorbance at 455 nm was measured to quantify the N_2H_4 concentration with a standard curve of hydrazine ($y = 0.58194x + 0.04348$, $R^2 = 0.999$).

Calculations of the conversion rate, FE, and NH_3 yield rate:

Equations of cathode reaction of NO_2^-RR:

$$NO_2^- + 6e^- + 8H^+ \rightarrow NH_4^+ + 2H_2O, \text{ in acidic media} \quad (1)$$

$$NO_2^- + 6e^- + 6H_2O \rightarrow NH_4^+ + 8OH^-, \text{ in neutral/alkaline media} \quad (2)$$

Equations of anode reaction:

$$4OH^- \rightarrow 2H_2O + O_2 + 4e^- \quad (3)$$

Possible overall reaction:

$$2NO_2^- + 6H_2O \rightarrow 3O_2 + 2\ NH_4^+ + 4OH^- \quad (4)$$

Equations of cathode reaction of NO_3^-RR:

$$NO_3^- + 8e^- + 10H^+ \rightarrow NH_4^+ + 3H_2O, \text{ in acidic media} \quad (5)$$

$$NO_3^- + 8e^- + 7H_2O \rightarrow NH_4^+ + 10OH^-, \text{ in neutral/alkaline media (6)}$$

FE toward NH_3 via NO_2^-RR was calculated by equation:

$$FE = 6 \times F \times ([NH_4^+] \times V / M_{NH4+}) / Q \times 100\% \text{ (7)}$$

FE toward NH_3 via NO_3^- reduction reaction (NO_3^-RR) was calculated by equation:

$$FE = (8 \times F \times [NH_4^+] \times V) / (M_{NH4+} \times Q) \times 100\% \text{ (8)}$$

NH_3 yield rate was calculated using the following equation:

$$NH_3 \text{ yield rate} = [NH_4^+] \times V / (M_{NH4+} \times t \times m_{cat.}) \text{ (9)}$$

Where F is the Faradic constant (96485 C mol^{-1}), $[NH_3]$ is the measured NH_3 concentration, V is the volume of electrolyte in the anode compartment (35 mL), M_{NH4+} is the molar mass of N NH_4^+, Q is the total quantity of applied electricity; t is the electrolysis time and $m_{cat.}$ is the loaded mass of catalyst.

The electrochemical impedance spectroscopy (EIS) was conducted at 0.3 V vs. RHE from 100 KHz to 0.1 Hz.

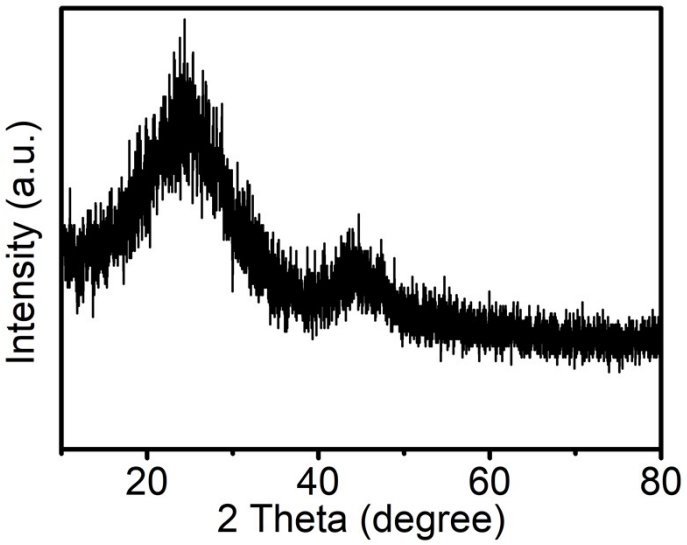

Fig. S1. XRD pattern of pure PP.

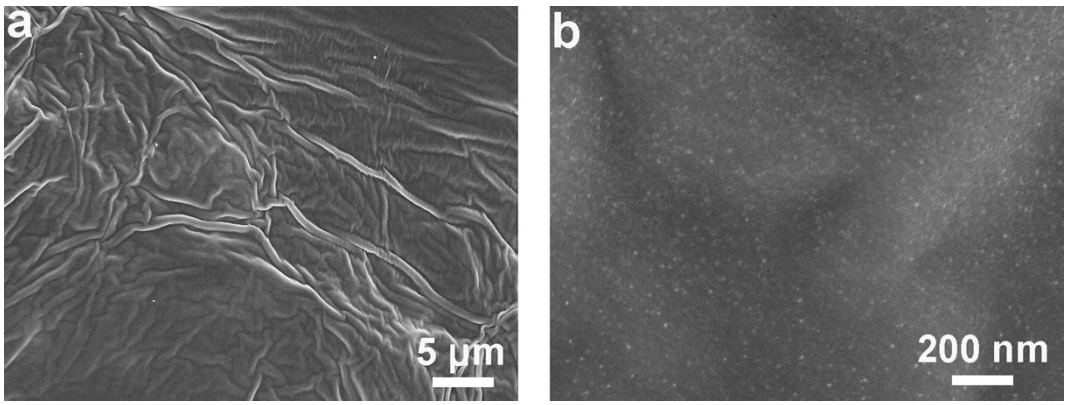

Fig. S2. SEM images of pure PP.

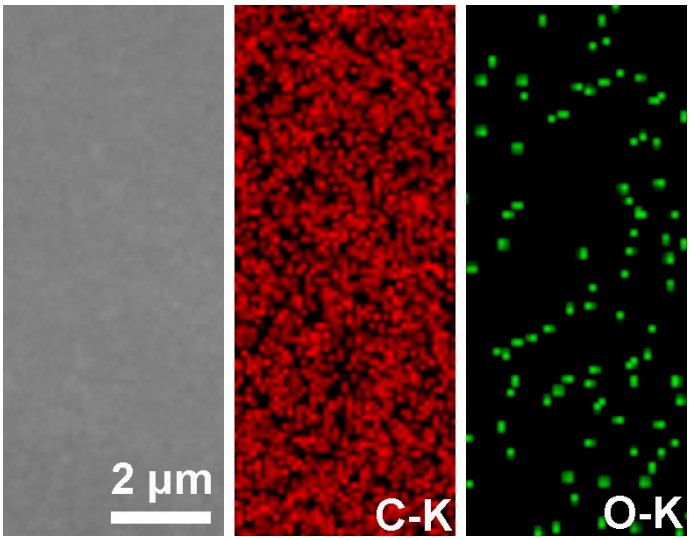

Fig. S3. SEM and EDX elemental mapping images of PP.

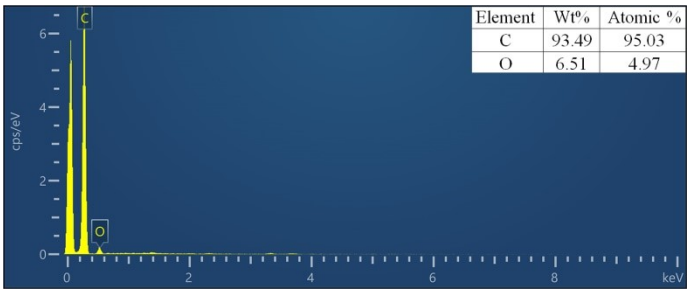

Fig. S4. EDX spectrum of PP.

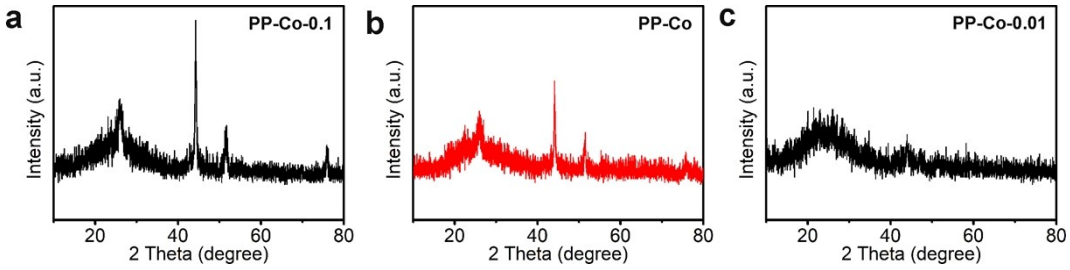

Fig. S5. XRD patterns of (a) PP-Co-0.1, (b) PP-Co, and (c) PP-Co-0.01.

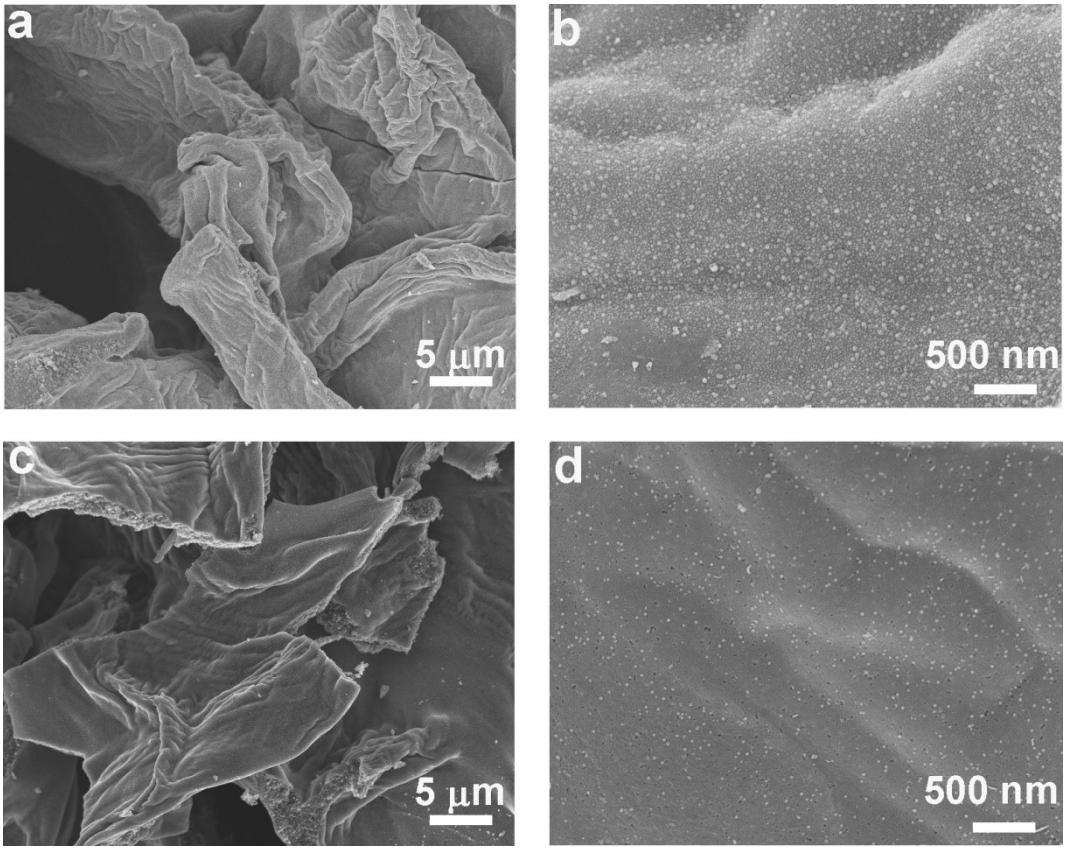

Fig. S6. SEM images of (a) and (b) PP-Co-0.1, (c) and (d) PP-Co-0.01.

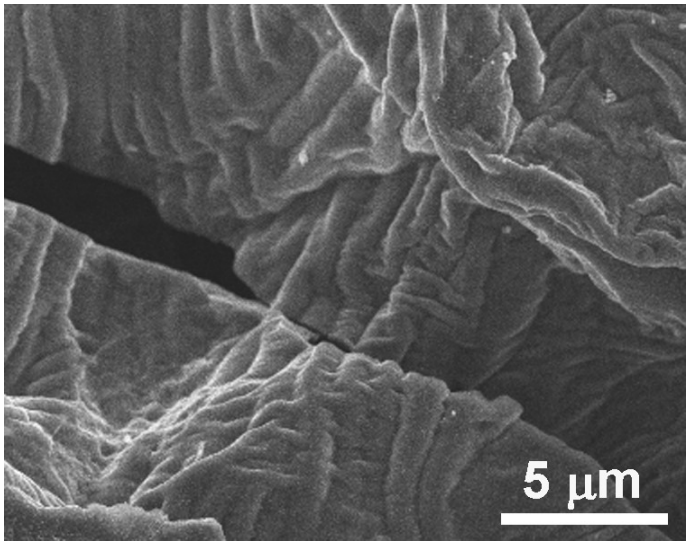

Fig. S7. SEM image of PP-Co.

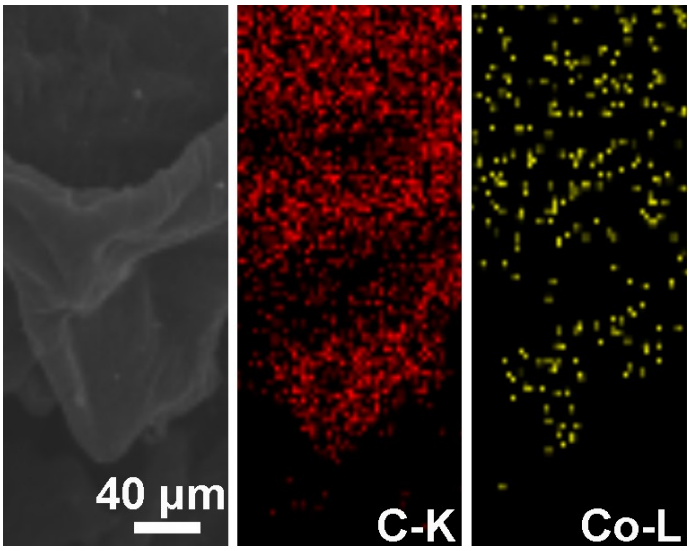

Fig. S8. SEM and EDX elemental mapping images of PP-Co.

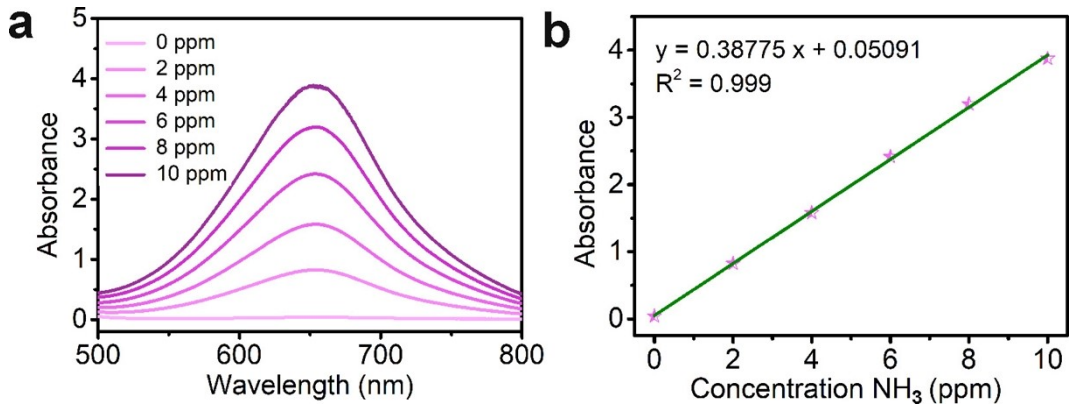

Fig. S9. (a) UV-Vis spectra and (b) corresponding calibration curve for determining NH_3.

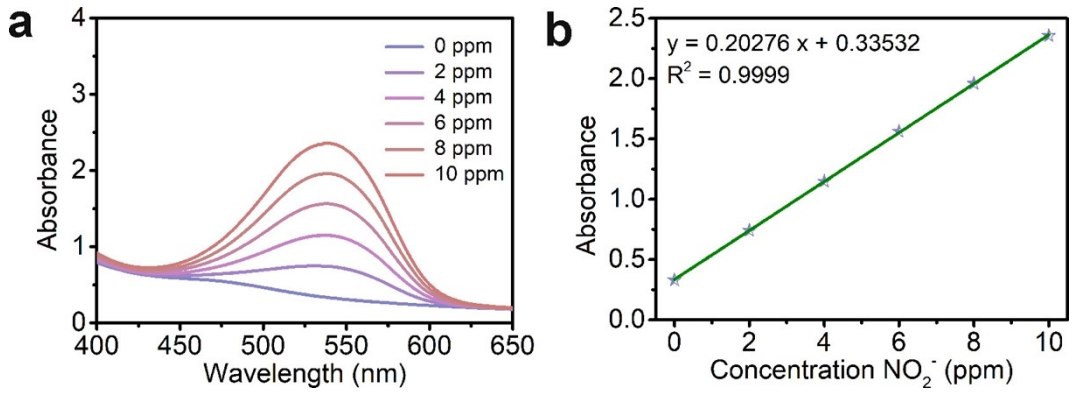

Fig. S10. (a) UV-Vis spectra and (b) corresponding calibration curve for determining NO_2^-.

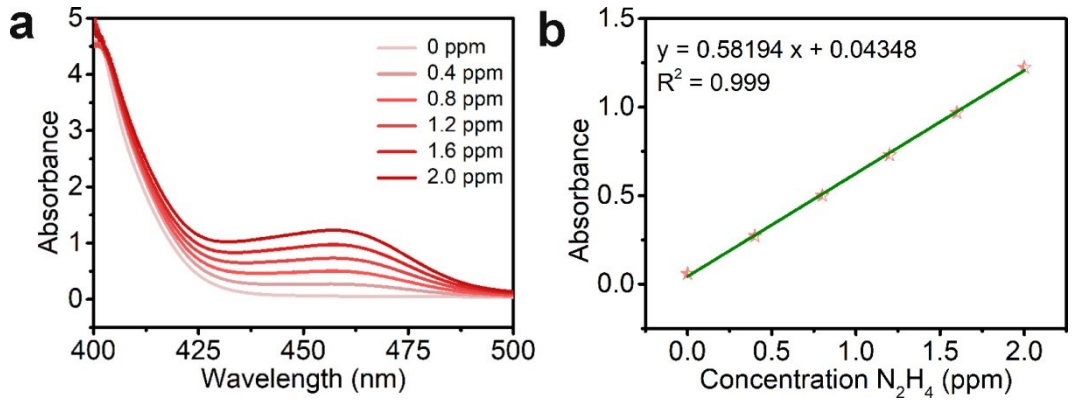

Fig. S11. (a) UV-Vis spectra and (b) corresponding calibration curve for determining N_2H_4.

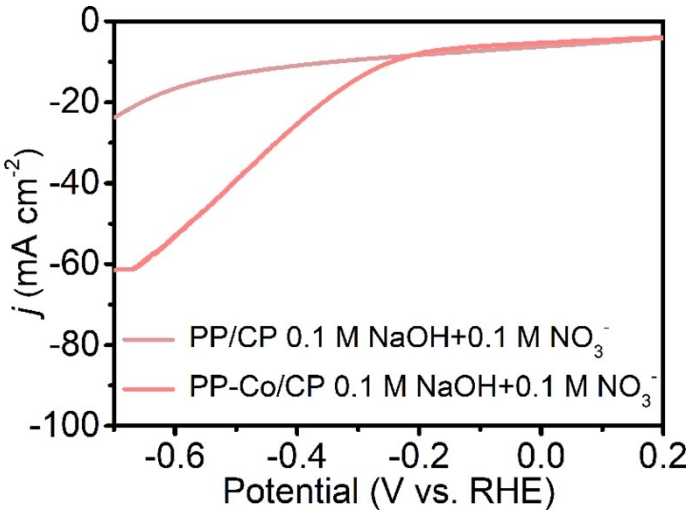

Fig. S12. LSV curves of pure PP/CP and PP-Co/CP tested in 0.1 M NaOH with 0.1 M NO_3^-.

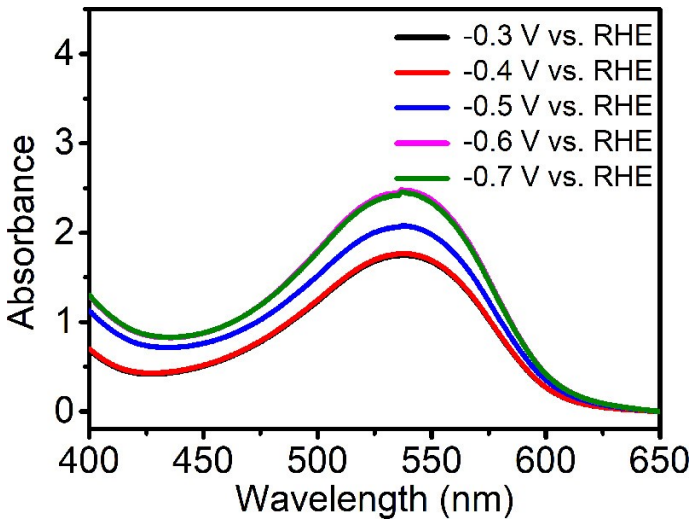

Fig. S13. UV-Vis spectra of electrogenerated NO_2^- for PP-Co/CP at different given potentials.

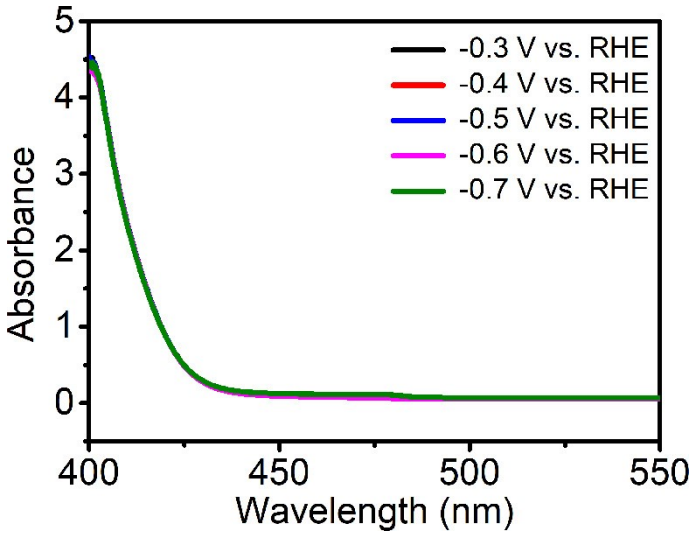

Fig. S14. UV-Vis spectra of electrogenerated N_2H_4 for PP-Co/CP at different given potentials.

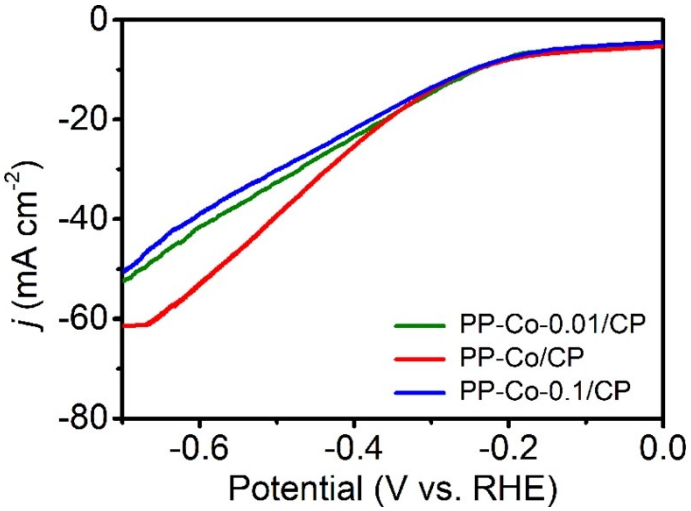

Fig. S15. LSV curves of PP-Co-0.01/CP, PP-Co/CP and PP-Co-0.1/CP tested in 0.1 M NaOH with 0.1 M NO_3^-.

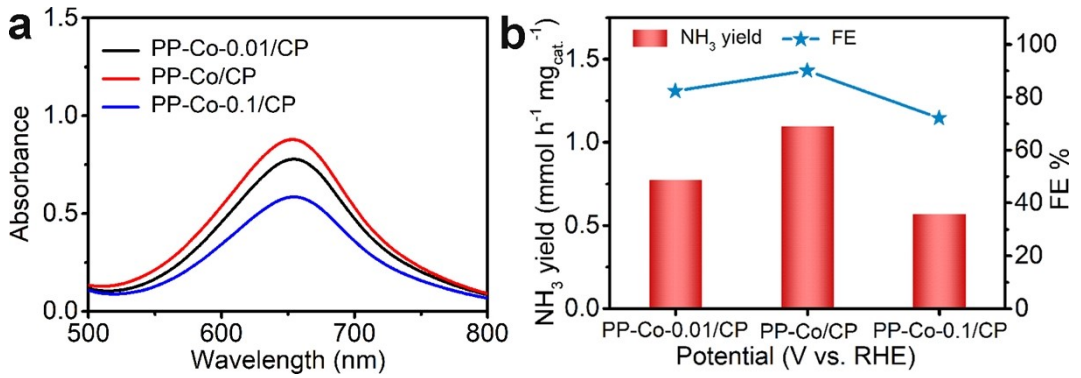

Fig. S16. (a) UV-Vis spectra of PP-Co-0.01/CP, PP-Co/CP, and PP-Co-0.1/CP for NO_3^-RR. (b) NH_3 yields and FEs of PP-Co-0.01/CP, PP-Co/CP and PP-Co-0.1/CP at −0.6 V.

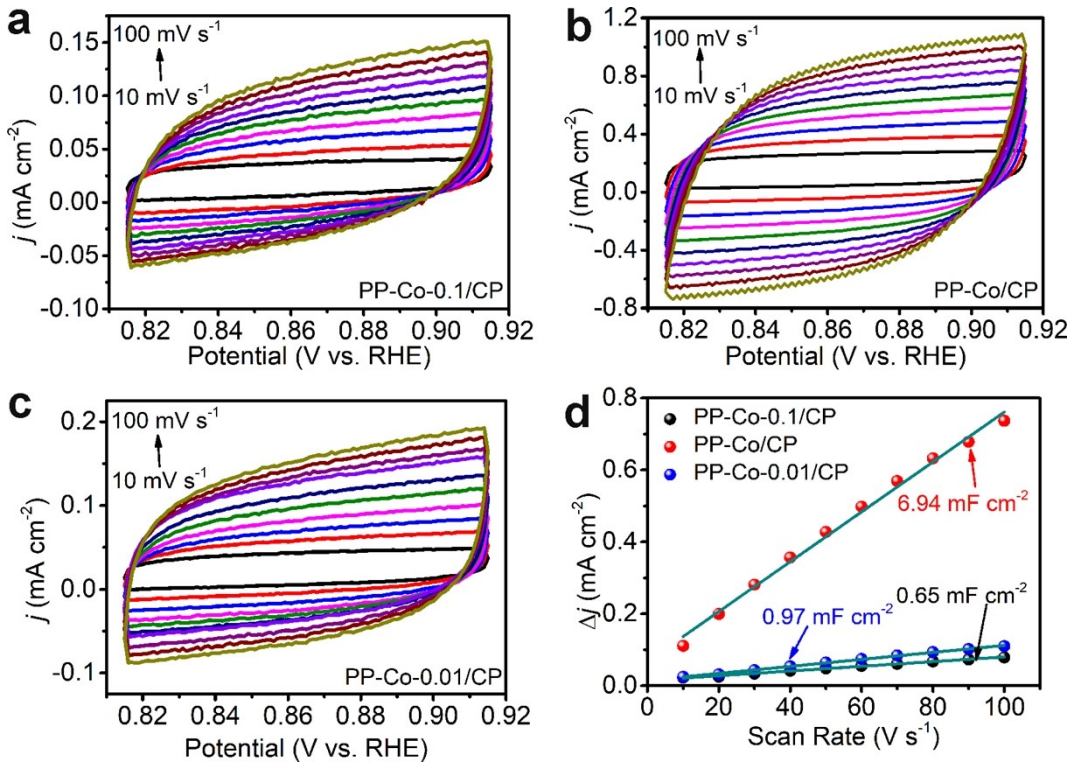

Fig. S17. CV curves for (a) PP-Co-0.1/CP, (b) PP-Co/CP, and (c) PP-Co-0.01/CP in the double layer region at scan rates of 10, 20, 30, 40, 50, 60, 70, 80, 90, and 100 mV s^{-1} in 0.1 M NaOH with 0.1 M NO_3^-. (d) Capacitive current as a function of scan rate at 0.865 V.

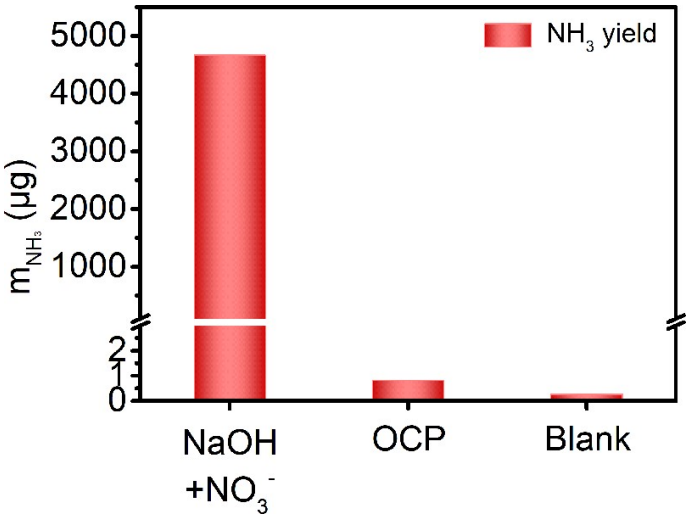

Fig. S18. Comparison of amount of produced NH_3 under three different conditions.

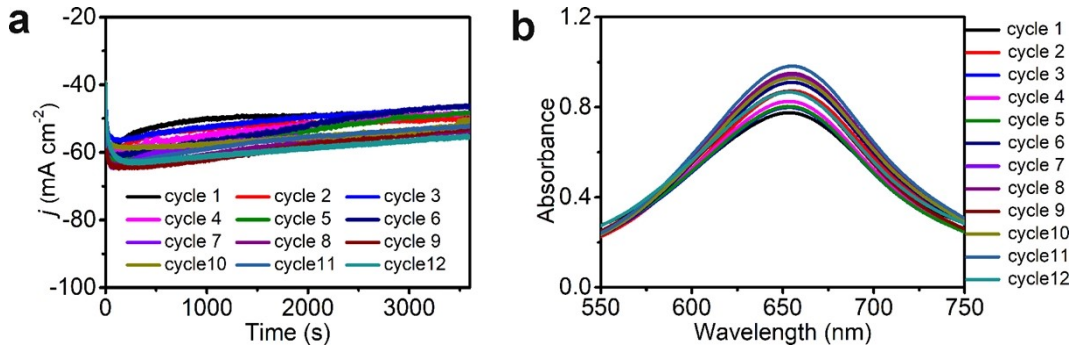

Fig. S19. (a) Time-dependent current density curves and (b) corresponding UV-Vis spectra of PP-Co/CP for electrogenerated NH_3 during recycling tests at −0.6 V vs. RHE in 0.1 M NaOH with 0.1 M NO_3^-.

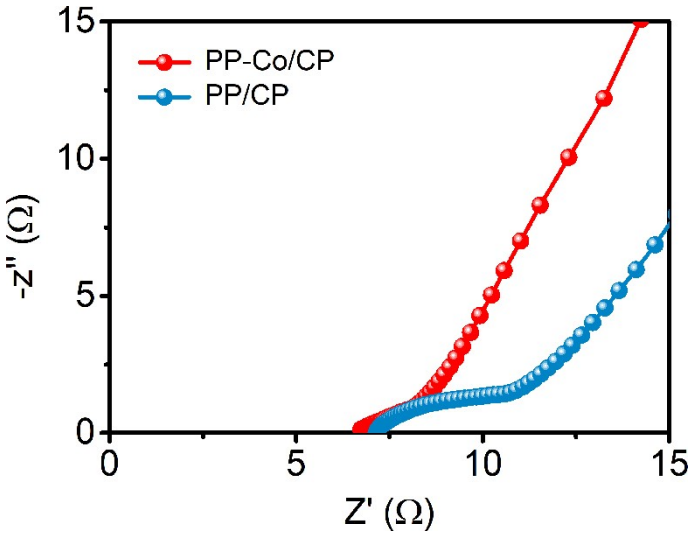

Figure S20. Nyquist plots of PP-Co/CP and PP/CP in 0.1 M NaOH with 0.1 M NO_3^-.

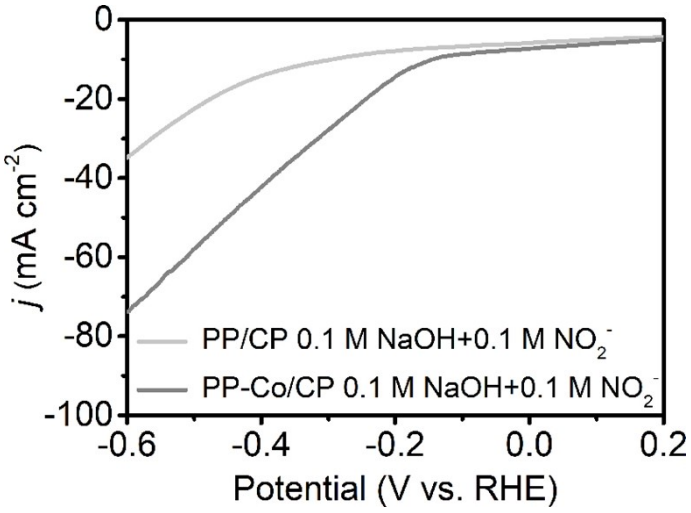

Fig. S21. LSV curves of pure PP/CP and PP-Co/CP tested in 0.1 M NaOH with 0.1 M NO_2^-.

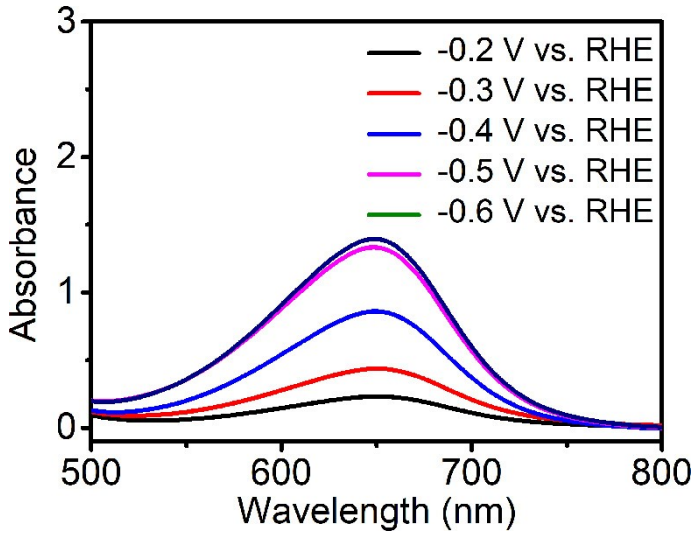

Fig. S22. UV-Vis spectra of PP-Co/CP for the NO_2^-RR at different given potentials.

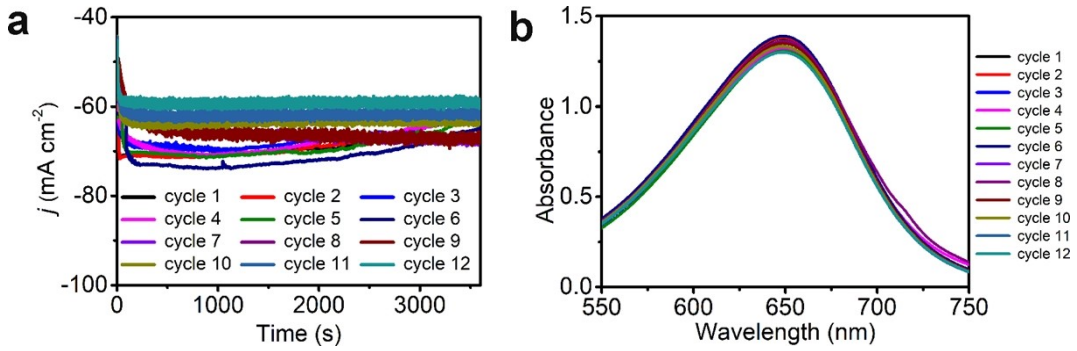

Fig. S23. (a) Time-dependent current density curves and (b) corresponding UV-Vis spectra of PP-Co/CP for electrogenerated NH_3 during recycling tests at −0.5 V vs. RHE in 0.1 M NaOH with 0.1 M NO_2^-.

Table S1. Comparison of catalytic performances of PP-Co/CP with other reported NO_3^-RR electrocatalysts.

Catalyst	Electrolyte	NH_3 yield rate@Potential (V vs. RHE)	FE@Potential (%@V vs. RHE)	Ref.
PP-Co/CP	0.1 M NaOH (0.1 M $NaNO_3$)	1.1 mmol h^{-1} $mg_{cat.}^{-1}$@–0.6	90.1@–0.6	This work
Cu/Cu_2O NWAs	0.5 M Na_2SO_4 (200 ppm NO_3^-)	4.1633 mg h^{-1} cm^{-2}@−0.85	95.8@−0.85	2
Cu nanosheets	0.1 M KOH (10 mM KNO_3)	0.023 mmol h^{-1} $mg_{cat.}^{-1}$@−0.15	99.7@−0.15	4
PTCDA/O-Cu	0.1 M PBS (500 ppm NO_3^-)	0.436±0.085 mg h^{-1} cm^{-2}@−0.4	85.9@−0.4	5
Fe SAC	0.10 M K_2SO_4 (0.5 M NO_3^-)	7.82 mg h^{-1} cm^{-2}@−0.85	75@−0.66	6
Co_3O_4@NiO HNTs	0.5 M Na_2SO_4 (200 ppm NO_3^-)	0.069 mmol h^{-1} $mg_{cat.}^{-1}$@−0.7	54.97@−0.7	7
TiO_{2-x}	0.5 M Na_2SO_4 (50 ppm NO_3^-)	0.765 mg h^{-1} cm^{-2}@−0.95	85@−0.95	8
Cu	1 M NaOH (0.1 M $NaNO_3$)	/	79	9
$Cu_{50}Ni_{50}$	1 M KOH (10 mM KNO_3)	/	84 ± 2	10
Ti/GC	KOH (~0.1 to 0.6 M NO_3^-)	/	82	11
Co/CoO NSA	0.1 M Na_2SO_4 (200 ppm NO_3^-)	3.3058 mg h^{-1} cm^{-2}@−0.65	93.8@−0.65	12
Ni_3B@$NiB_{2.74}$	0.1 M KOH (0.01 M NO_3^-)	0.194 mmol h^{-1} cm^{-2}@−0.3	100@−0.3	13
FC	0.05 M H_2SO_4 (200 ppm KNO_3)	0.0238 mmol h^{-1} $mg_{cat.}^{-1}$@−0.7	20@−0.65	14

PCNV-600	0.5 M Na_2SO_4 (100 ppm NO_3^-–N)	0.033 mmol h^{-1} $mg_{cat.}^{-1}$@−0.95	29.96@−0.95	15
In-S-G	1 M KOH (0.1 M KNO_3)	0.22 mmol h^{-1} $mg_{cat.}^{-1}$@−0.7	75@−0.5	16
CoP NRs	0.5 M Na_2SO_4 (50 mM $NaNO_3$)	1.77 mmol h^{-1} $mg_{cat.}^{-1}$@−0.5	97.1@−0.5	17

Table S2. Comparison of catalytic performances of PP-Co/CP with other reported NO_2^-RR electrocatalysts.

Catalyst	Electrolyte	NH_3 yield rate@Potential (V vs. RHE)	FE@Potential (%@V vs. RHE)	Ref.
PP-Co/CP	0.1 M NaOH (0.1 M $NaNO_2$)	1.68 mmol h^{-1} $mg_{cat.}^{-1}$@–0.5	86.8@–0.5	This work
Ni-NSA-V_{Ni}	0.2 M Na_2SO_4 (200 ppm NO_2^-)	4.01 mg h^{-1} cm^{-2}@−0.55	88.9@−0.55	18
CoP NA/TM	0.1 M PBS (500 ppm NO_2^-)	2.26 mg h^{-1} cm^{-2}@−0.2	90@−0.2	19
Ni_2P/NF	0.1 M PBS (200 ppm NO_2^-)	2.69 mg h^{-1} cm^{-2}@−0.85	90@−0.66	20
Co-P/TP	0.2 M Na_2SO_4 (200 ppm NO_2^-)	0.66 mg h^{-1} cm^{-2}@−0.6	93.3@−0.2	21
Cu_3P NA/CF	0.1 M PBS (0.1 M NO_2^-)	1.63 mg h^{-1} cm^{-2}@−0.5	91.2@−0.5	22

References

1 D. Zhu, L. Zhang, R. E. Ruther and R. J. Hamers, *Nat. Mater.,* 2013, **12**, 836–841.

2 Y. Wang, W. Zhou, R. Jia, Y. Yu and B. Zhang, *Angew. Chem., Int. Ed.,* 2020, **59**, 5350–5354.

3 G. W. Watt and J. D. Chrisp, *Anal. Chem.,* 1952, **24**, 2006–2008.

4 X. Fu, X. Zhao, X. Hu, K. He, Y. Yu, T. Li, Q. Tu, X. Qian, Q. Yue, M. Wasielewski and Y. Kang, *Appl. Mater. Today,* 2020, **19**, 100620.

5 G. Chen, Y. Yuan, H. Jiang, S. Ren, L. Ding, L. Ma, T. Wu, J. Lu and H. Wang, *Nat. Energy,* 2020, **5**, 605–613.

6 Z. Wu, M. Karamad, X. Yong, Q. Huang, D. A. Cullen, P. Zhu, C. Xia, Q. Xiao, M. Shakouri, F. Chen, J. Y. Kim, Y. Xia, K. Heck, Y. Hu, M. S. Wong, Q. Li, I. Gates, S. Siahrostami and H. Wang, *Nat. Commun.,* 2021, **12,** 2870.

7 Y. Wang, C. Liu, B. Zhang and Y. Yu, *Sci. China Mater.,* 2020, **63**, 2530–2538.

8 R. Jia, Y. Wang, C. Wang, Y. Ling, Y. Yu and B. Zhang, *ACS Catal.,* 2020, **10,** 3533−3540.

9 D. Reyter, G. Chamoulaud, D. Bélanger and L. Roué, *J. Electroanal. Chem.,* 2006, **596**, 13–24.

10 Y. Wang, A. Xu, Z. Wang, L. Huang, J. Li, F. Li, J. Wicks, M. Luo, D. H. Nam, C. Tan, Y. Ding, J. Wu, Y. Lum, C. T. Dinh, D. Sinton, G. Zheng and E. H. Sargent, *J. Am. Chem. Soc.,* 2020, **142**, 5702–5708.

11 J. M. McEnaney, S. J. Blair, A. C. Nielander, J. A. Schwalbe, D. M. Koshy, M. Cargnello and T. F. Jaramillo, *ACS Sustainable Chem. Eng.,* 2020, **8**, 2672−2681.

12 Y. Yu, C. Wang, Y. Yu, Y. Wang and B. Zhang, *Sci. China Chem.,* 2020, **63**, 1469–1476.

13 L. Li, C. Tang, X. Cui, Y. Zheng, X. Wang, H. Xu, S. Zhang, T. Shao, K.

Davey and S. Qiao, *Angew., Chem. Int. Ed.,* 2021, **60**, 14131–14137.

14 Y. Li, S. Xiao, X. Li, C. Chang, M. Xie, J. Xu and Z. Yang, *Mater. Today Phys.,* 2021, **19**, 100431.

15 Y. Huang, J. Long, Y. Wang, N. Meng, Y. Yu, S. Lu, J. Xiao and B. Zhang, *ACS Appl. Mater. Interfaces,* 2021, **13**, 54967–54973.

16 F. Lei, W. Xu, J. Yu, K. Li, J. Xie, P. Hao, G. Cui and B. Tang, *Chem. Eng. J.,* 2021, **426**, 131317.

17 Q. Hong, J. Zhou, Q. Zhai, Y. Jiang, M. Hu, X. Xiao, S. Li and Y. Chen, *Chem. Commun.,* 2021, **57**, 11621–11624.

18 C. Wang, W. Zhou, Z. Sun, Y. Wang, B. Zhang and Y. Yu, *J. Mater. Chem. A,* 2021, **9**, 239–243.

19 G. Wen, J. Liang, Q. Liu, T. Li, X. An, F. Zhang, A. A. Alshehri, K. A. Alzahrani, Y. Luo, Q. Kong and X. Sun, *Nano Res.,* 2022, **15**, 972–977.

20 G. Wen, J. Liang, L. Zhang, T. Li, Q. Liu, X. An, X. Shi, Y. Liu, S. Gao, A. M. Asiri, Y. Luo, Q. Kong and X. Sun, *J. Colloid. Interf. Sci.,* 2022, **606**, 1055–1063.

21 Z. Li, G. Wen, J. Liang, T. Li, Y. Luo, Q. Kong, X. Shi, A. M. Asiri, Q. Liu and X. Sun, *Chem. Commun.,* 2021, **57**, 9720–9723.

22 J. Liang, B. Deng, Q. Liu, G. Wen, Q. Liu, T. Li, Y. Luo, A. A. Alshehri, K. A. Alzahrani, D. Ma and X. Sun, *Green Chem.,* 2021**, 23**, 5487–5493.